PROCEEDINGS OF SPIE

SPIEDigitalLibrary.org/conference-proceedings-of-spie

Enhanced diagnostic of skin conditions by polarized laser speckles: phantom studies and computer modeling

Lioudmila Tchvialeva, Tim K. Lee, Igor Markhvida, Haishan Zeng, Alexander Doronin, et al.

Lioudmila Tchvialeva, Tim K. Lee, Igor Markhvida, Haishan Zeng, Alexander Doronin, Igor Meglinski, "Enhanced diagnostic of skin conditions by polarized laser speckles:
phantom studies and computer modeling," Proc. SPIE 8926, Photonic Therapeutics and Diagnostics X, 89260X (4 March 2014); doi: 10.1117/12.2040192

SPIE.

Event: SPIE BiOS, 2014, San Francisco, California, United States

Enhanced diagnostic of skin conditions by polarized laser speckles: phantom studies and computer modeling

Lioudmila Tchvialeva[a], Tim K. Lee[♣a,b,c], Igor Markhvida[a], Haishan Zeng[a,b], Alexander Doronin[d], and Igor Meglinski[d]

[a] Photomedicine Institute, Department of Dermatology and Skin Science, Vancouver Coastal Health Research Institute and University of British Columbia, Vancouver, Canada

[b] Departments of Cancer Control Research and Integrative Oncology, BC Cancer Agency, Vancouver, Canada

[c] School of Computing Science, Simon Fraser University, Burnaby, Canada

[d] Jack Dodd Center for Quantum Technologies, Department of Physics, University of Otago, Dunedin, New Zealand

ABSTRACT

The incidence of the skin melanoma, the most commonly fatal form of skin cancer, is increasing faster than any other potentially preventable cancer. Clinical practice is currently hampered by the lack of the ability to rapidly screen the functional and morphological properties of tissues. In our previous study we show that the quantification of scattered laser light polarization provides a useful metrics for diagnostics of the malignant melanoma. In this study we exploit whether the image speckle could improve skin cancer diagnostic in comparison with the previously used free-space speckle. The study includes skin phantom measurements and computer modeling. To characterize the depolarization of light we measure the spatial distribution of speckle patterns and analyse their depolarization ratio taken into account radial symmetry. We examine the dependences of depolarization ratio vs. roughness for phantoms which optical properties are of the order of skin lesions. We demonstrate that the variation in bulk optical properties initiates the assessable changes in the depolarization ratio. We show that image speckle differentiates phantoms significantly better than free-space speckle. The results of experimental measurements are compared with the results of Monte Carlo simulation.

Keywords: polarization, laser speckle imaging, surface roughness, depolarization ratio, skin phantom, melanoma, skin cancer, Monte Carlo modelling

1. INTRODUCTION

The incidence of the skin melanoma the, the most commonly fatal form of skin cancer, is increasing faster than any other potentially preventable cancer. The World Health Organisation proposes that early detection of cancer is crucial in cancer management in primary care settings. Laser light scattered by biological tissue carries information about its morphology and can be used to detect the structural abnormalities associated with various decease. A number of recent scattering-based techniques including optical/near-infrared spectroscopy, optical diffuse tomography utilize the light intensity. The use of light coherence and polarization is the next logical step that is currently under active development[1]. The preserving of initial polarization in backscattered light[2] and the strong dependence of the residual polarization on the morphological structure of the probed tissue[3] allow for the development of the simple polarimetric methods for optical diagnostics[4,5]. Modification of polarization during light scattering in tissue is quite complicated. In each point (or elementary volume) light has its own state of polarization resulted from interference of many waves. This spatial random distribution of polarization is called polarization speckle and is a subject of statistical optics[6,7]. The results of our recent study[8] demonstrate that polarization speckle has a great potential for skin cancer detection.

♣ Correspondence: Vancouver Coastal Health Research Institute and University of British Columbia, Department of Dermatology and Skin Science, Photomedicine Institute, Vancouver, Canada; E-mail: tlee@bccrc.ca; Phone: 604-675-8053; Fax: 604-675-8180.

Photonic Therapeutics and Diagnostics X, edited by Bernard Choi, et al., Proc. of SPIE
Vol. 8926, 89260X · © 2014 SPIE · CCC code: 1605-7422/14/$18 · doi: 10.1117/12.2040192

In current paper we examine the possibility to improve the skin cancer diagnostics by the imaging speckle set-up instead the previously used free-speckle scheme. We hypothesize that resolving the distribution of depolarization over the skin surface we will get advantage of the spatial polarization features. Simultaneous investigation of polarization in many points is a challenging experimental task. Light depolarization due to scattering on the rough surface[9] could affect the preservation of polarization and should be addressed. Taking rough surface in to consideration adds one more level of complexity[10]. In such conditions we found the best strategy to explore the light depolarization in skin lesions is a Monte-Carlo (MC) simulation combined with experiments on rough durable phantoms with controllable optical parameters simulating human skin. For this purpose we design two semi-transparent solid silicone phantoms with refraction index, absorption, scattering and roughness of the order of human skin. We measure the mean depolarization ratio of backscattered light for two phantoms using imaging and free-space speckle set-ups varying phantom's roughness. Then we compare the performance of both set-ups calculating the coefficient of variation between two phantoms. We find that image device differentiates two phantoms significantly better than used in our recent clinical trial free-space device. The experimental data are compared with the results of corresponding computational studies by MC model developed in house[11-15].

2. MATERIAL AND METHODS

2.1 Skin Phantoms

To create the desired human skin phantoms we choose Smooth-On brand MoldMax® 10T silicone that comes as a viscous resin, accompanied by a curative that causes the silicone to cure at room temperature (the refraction index n is about 1.41). We use SILC-PIG® pigments as absorbing particles (Smooth-On, Inc, USA). The liquid pigments come in nine different colors and create a colored homogeneous solution when mixed with silicone resin. Using proper pigments concentrations we can imitate the color of a human skin. Each silicone phantom surface was made as a replica from metal standard (Microshurf #334, Rubert + Co Ltd.) to have the same series of rough surfaces in the range from 2.5 to 65.2 μm, which are of the order of human skin roughness. We have measured the skin's root mean square (h_{rms}) roughness variation in the range between 10 - 40 μm[16]. Every one rough phantom has dimensions 20 mm × 10 mm ×10 mm. The phantom roughness was confirmed by WYKO NT1100 optical profilometer (Veeco,USA) with vertical resolution 0.05 μm, lateral resolution 0.5 μm and a standard error 10%. . The optical properties μ_s' and μ_a, and g of the produced phantoms where obtained using a red diode laser (B&WTek Flex, 5 mW, λ=663 nm), the integration sphere technique[17] and a ballistic photon detection set-up[18]. Multiple measurements including transmittance, reflectance and unchartered transmittance values were inputted in the Inverse Adding-Doubling software downloaded from[17]. The obtained optical properties of the phantoms are presented in Table 1 along with their standard errors. Comparing values from Table 1 to literature data on skin optical properties[19-22] that the produced skin phantoms have bulk optical properties in the range of human skin. Therefore we can classify the fabricated phantoms as rough skin phantoms.

Table 1. The bulk optical properties of phantoms and skin tissue lesions (wavelength 633 nm).

	μ_a, mm^{-1}	μ_s', mm^{-1}
Phantom I - Dark	0.44±0.04	0.51±0.05
Phantom II - Light	0.26±0.03	1.29±0.13
Normal skin (*in vivo*)[22]	0.026	1.13
Skin dermis (*in vitro*)[23]	0.15	2.78
Skin epidermis (*in vitro*)[23]	0.26	4.48
Basal Cell Carcinoma (*in vivo*)[22]	0.051	1.90
Basal Cell Carcinoma(*in vitro*)[23]	0.14	2.59
Squamous Cell Carcinoma (*in vivo*)[22]	0.063	1.08
Squamous Cell Carcinoma(*in vitro*) [23]	0.11	1.71
Malignant Melanoma (*in vivo*)[22]	0.067	1.91
Seborrheic Keratosis (*in vivo*)[22]	0.049	1.61

2.1 Laser speckle imaging set-up

The experimental geometry of free-space speckle device was described in Ref.8. The new image speckle set up is shown in Figure 1. Phantom surfaces were illuminated sequentially by white diode light producing the gray image and a fiber-coupled red diode laser (λ=663 *nm*, 5 *mW*, Flex, B&WTek Inc). The angle of incidence was in the normal direction to the skin surface. The backscattered signals were observed in the specular direction. An optical scheme had a magnification 1.3 and field of view 7 *mm* × 5 *mm*. The input-output polarizes control the polarization of the images. The imageing speckle pattern was acquired simultaneously by two grayscale CCD cameras (Matrix Vision GmbH, mvBlueFOX-M124G- 8bit and mvBlueFOX-M224G- 10 bit) with CCTV lens (50 *mm* F/1.4, Pentax Inc). The distance between the surface and the CCD matrixes (pixel size is about 4.4 *μm*) was 157 *mm*. The average red speckle size is about 12 *μm* under our set up. Figure 1 also shows the image of laser beam which size is about 300 *μm* (1); the prospective dermoscopy image (2) we plan to get by colour CCD cameras, as for now we use the lesion image for the beam alignment; the typical backscattered light spot on a rough phantom in parallel (3) and perpendicular directions (4) with respect to the polarization of the incident light.

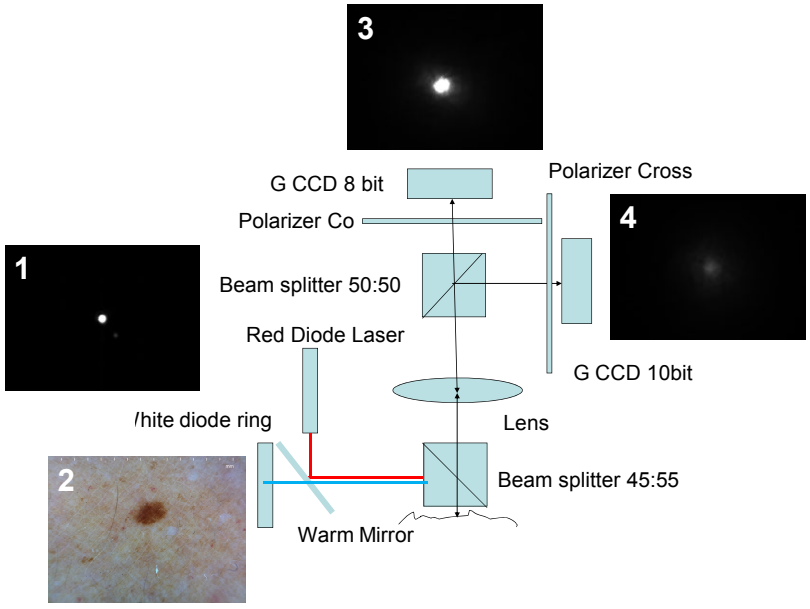

Figure 1. Schematic presentation of the laser speckle imaging experimental system.

2.3 Signal processing

Two free-speckle speckle patterns $I_{II}(x,y)$ and $I_{\perp}(x,y)$ (parallel- and perpendicular-polarized) were registered simultaneously. Signal processing included dark signal subtraction and matching the images in a way providing pixel-to-pixel correspondence. A spatial distribution of depolarization ratio $D(x,y)$ is then calculated from the two speckle patterns[8]:

$$D(x,y)=\frac{I_{II}(x,y)-I_{\perp}(x,y)}{I_{II}(x,y)+I_{\perp}(x,y)}. \quad (1)$$

As shown earlier this two-dimensional random field $D(x,y)$ is spatially stationary and therefore can be characterized by the probability density function (pdf)[8]. For routine experimental purpose the pdf is not practical to be used, and that is why we represent polarization speckle field by its' statistical metrics – moments. The first order statistical moment of the in the polarization speckle pattern polarization ratio $D(x,y)$ is calculated based on the following equation:

$$\overline{D}=\frac{1}{N}\sum_{1}^{N}|D(x,y)|, \quad (2)$$

where N denotes the total number of pixels.

In contrast with the statistically uniform speckle pattern (Gaussian distribution) formed in free-space the observed image speckle pattern is non-uniform and has a circular symmetry (see Figure1-3 and 1-4). This is due to the use of narrow laser beam (~ 300 microns in diameter) and wide field of view projected on CCD cameras (7 *mm* × 5 *mm*).

An example of typical speckle pattern distribution $I(x,y)$ measured with the experimental set-up described above is presented in Figure 2.

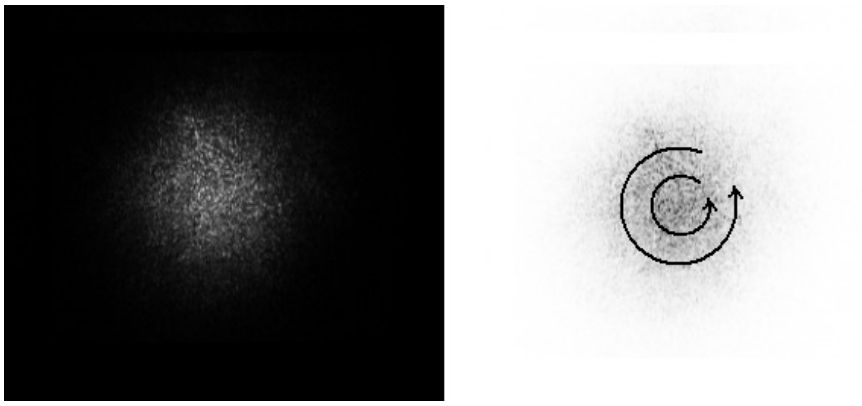

Figure 2: The original image of near surface speckle pattern (left), and the negative of the same image with the arrows showing radial averages (right).

Typically, the analysis of speckle patterns is based on the first-order statistics of surface speckle pattern. The speckle image of the rough surface has a less contrast than smoother surface. This is due to that the light losses it's coherence after scattering, whereas the speckle contrast is a metric of light coherence. Speckle pattern presented in Figure 2 could be satisfied the ergodic stochastic process. However, a small number of speckles turn out insufficient to get a good statistical data. In addition the weak intensity and its fluctuations produce very unstable spatial intensity distribution that significantly limits the area of measurements covering mainly the central region. To treat this speckle pattern properly in a way to get appropriate statistical data the development of a new signal processing approach is required.

Speckle correlation approach is the second-order statistic method and is based on the correlation between different speckle patterns that can be performed, e.g. by radial averaging as shown at the inverted laser speckle image presented in Figure 2. However, the intensity taken along the circle line centered in picture (see Figure 2) disclosures the stationary property. As the statistical properties of the speckles shouldn't depend on the azimuth, the spatial averaging in (2) then can be replaced with the angle averaging.

Thus, the following procedure of signal processing has been applied:

- Finding the centre of the pattern.
- Selection of the initial radius R of circle line.
- Reading the values of intensity of the detected scattered light along the selected circle line.
- Counting the mean value dataset $<I(R)>$.
- Increase radius R of the circle line and repeat the actions above, starting from step 1.
- Continue the procedure till the radius reaches the boundary of image.

Finally, by collecting the radial distribution of average intensities for co- $<I_{\parallel}(R)>$ and cross- $<I_{\perp}(R)>$ polarized light the radial distribution of depolarization ratio is defined as:

$$D(R) = \frac{< I_{\parallel}(R) > - < I_{\perp}(R) >}{< I_{\parallel}(R) > + < I_{\perp}(R) >}. \tag{3}$$

3. RESULTS AND DISCUSSION

3.1 Results of experiment

Figure 3 presents the radial distributions of the intensity $<I_{||}(R)>$ and depolarization ratio.

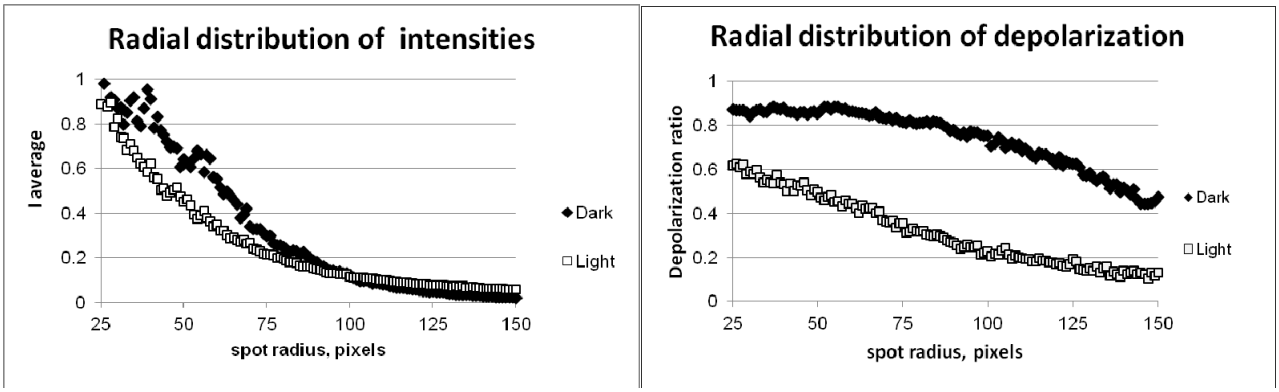

Figure 3. The radial distributions of mean normalized intensity $<I_{||}(R)>$ and ratio of depolarization for phantom I (Light) and phantom II (Dark) with optical properties, presented in Table 1. Both phantoms have roughness 34 microns.

Each laser speckle pattern reveals almost circular symmetry with the intensity gradually reduced from the center towards the edges. As one can see the intensity and the depolarization ratio calculated by (3) also reduces towards the edges of the detected spot (see Figure 3(a) and (b)). The comparison of radial distributions for two skin phantoms presented in Figure 3 clearly shows that the depolarization ratio is a stronger parameter and can be used for the quantitative measure of variations of the samples.

3.2 Monte Carlo modeling

Owing to a wide range of actual probing conditions and a very complex composite structure of human skin that is a primary aim of current study, no general analytical solution is available that can simulate the detected scattered co- and cross- polarized light and its interaction with rough surface and superficial tissues. Therefore, we utilized a recently developed object oriented MC model[12,24] that also allows simulate the propagation and scattering of coherent polarized light in complex tissue-like scattering medium

The general description of the polarized MC algorithm is well known and widely described elsewhere[11-15]. Briefly, a photon packet is first initialized with a weight of 1 and injected into a modelling semi-infinite scattering and absorbing medium. The random path length l a photon packet goes for a step i is given by

$$l = -\frac{\ln \xi}{\mu_s}, \tag{4}$$

where ξ is the computer-generated random number, uniformly distributed in the interval [0,1], μ_s is the scattering coefficient. Henyey-Greenstein phase function[25] is used in the simulation to describe scattering indicatrix, and the parameter g is defined as the average $\cos\theta$ for a given phase function.

Internal reflections on medium boundary are taken into account by splitting the photon packet into reflected and transmitted parts as suggested in[26]. The weights of these parts are attenuated according to the Fresnel reflection coefficients:

$$W = W_0(1 - R_0(\alpha))\prod_{p=1}^{M} R_p(\alpha). \tag{5}$$

Here, W_0 is the initial weight of the photon packet, M is the number of times the photon packet experiences a partial reflection on medium boundary, $R(\alpha)$ is the Fresnel reflection coefficient for the p-th photon-boundary interaction, $R_0(\alpha)$ is the Fresnel reflection coefficient for the initial photon-boundary interaction, where the photon packet enters the medium, α is the angle of incidence on the medium boundary[26]. The details of the rough surface formation are given in Ref.27 and not presented in current report. The simulation of the photon tracing within the medium is stopped when a photon packet has been scattered more than 10^4 times and does not depend on absorption. The counting of normalized skin spectra $I(\lambda)$ is based on the microscopic Beer–Lambert law and defined as follows[26]:

$$I(\lambda) = \frac{1}{N_{ph} W_0} \sum_{j=1}^{N_{ph}} W_j \exp(-\sum_{i=1}^{Kj} \mu_{ai}(\lambda) l_i), \quad (6)$$

where W_j is the final weight of the j-th photon packet defined by (5), K_j is the total number of scattering events for the j-th photon packet, μ_{ai} and l_i are the medium-local absorption coefficient and the path length of photon packet at i-th step, respectively[26]. The total number of the photon packets N_{ph} typically used in simulation is ~ 10^8-10^9.

The Bethe–Salpeter equation (BSE)[28] describes a transfer of pair of complex-conjugated fields, incident into point of source R_S with the wave vector k_i and outgoing in the detecting point R_D with the wave vector k_D. Iterating the BSE presents the intensity of scattered light as the series in scattering orders, where the first term describes the single scattering, second term describes two scattering events, *etc*. Within the MC approach the scattering intensity is also presented as the sum of scattering orders. Thus, by an analogy to the iterative procedure of the solution of BSE in our MC model the polarization track in multiple scattering medium is performed in terms of a polarization vector $\vec{P}$ that is undergoing a sequence of transformations after each scattering event. The trajectories of the photon packet are weighted (W) in accordance with the polarization state, and the polarization vector of the scattered wave $\vec{P}_i$ is transformed upon the i-th scattering event, as[13]:

$$\vec{P}_i = -\vec{e}_i \times [\vec{e}_i \times \vec{P}_{i-1}] = [\hat{I} - \vec{e}_i \otimes \vec{e}_i] \vec{P}_{i-1}, \quad (7)$$

where $\vec{e}_i$ is the unite vector aligned along the trajectory element of a photon packet after the i^{th} scattering event. Tensor $\mathbf{S}_i = [\hat{I} - \vec{e}_i \otimes \vec{e}_i]$ is presented as:

$$\mathbf{S}_i = \begin{pmatrix} 1 - e_{iX}^2 & -e_{iX} e_{iY} & -e_{iX} e_{iZ} \\ -e_{iX} e_{iY} & 1 - e_{iY}^2 & -e_{iY} e_{iZ} \\ -e_{iX} e_{iZ} & e_{iX} e_{iZ} & 1 - e_{iZ}^2 \end{pmatrix} \quad (8)$$

and, thus, the chain of projection operators $\mathbf{S}_i$ transforms the initial polarization $\vec{P}_0$ upon a sequence of n scattering events to the final polarization $\vec{P}_n$, i.e.:

$$\vec{P}_n = \mathbf{S}_n \mathbf{S}_{n-1} ... \mathbf{S}_1 \vec{P}_0. \quad (9)$$

Consequently, propagation of co- and cross-polarized components of electromagnetic field in the medium is described along the same trajectories obtained for the scalar field. To link the scalar and vector nature of electromagnetic fields according the optical theorem[29] the Rayleigh factor is taken into account at every scattering event for electromagnetic field[14,30]:

$$\Gamma = \frac{2}{1 + cos^2 \theta} \quad (10)$$

Thus, in the final expression for the co- ($I_{\parallel}$) and cross- ($I_{\perp}$) polarized intensities of backscattered light is:

$$\begin{aligned} I_{XX}(x,y) &= \tfrac{1}{N_{ph}} \sum_{j=1}^{N_{ph}} \left(W_j \Gamma^{n_j} P_{XX_j}^2 \exp\left(-\mu_a L_j\right) \right) \\ I_{\perp}(x,y) &= \tfrac{1}{N_{ph}} \sum_{j=1}^{N_{ph}} \left(W_j \Gamma^{n_j} P_{XY_j}^2 \exp\left(-\mu_a L_j\right) \right) \end{aligned} \quad (11)$$

where N_{ph} is the total number of the detected photon packets, n is the number of scattering events experienced by j-th photon packet at its trajectory L from point of incidence R_S to the detector R_D. Further details can be found in Refs: 11-15,30.

3.3 Monte Carlo modeling

The results of simulation including for co- $I_{\parallel}(x,y)$ and cross- $I_{\perp}(x,y)$ polarized light and the depolarization ration DR for the two modelling media with the same optical properties and roughness as presented in Figure 4.

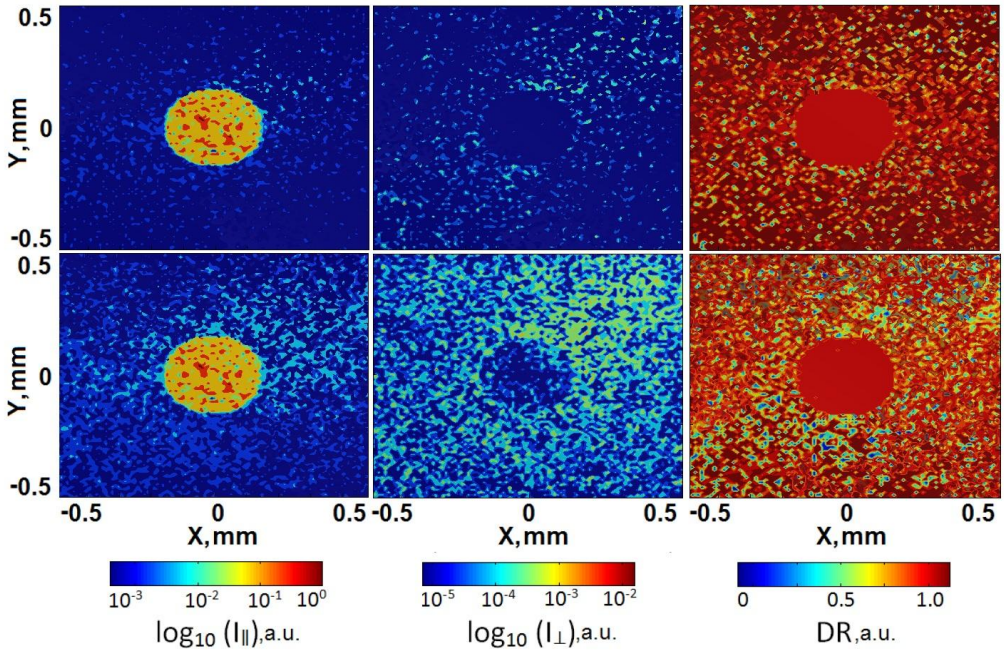

Figure 4. Spatial distributions of normalized co- $I_{\parallel}$ and $I_{\perp}$cross- polarized intensities of the backscattered light and the depolarization ratio for dark phantom (upper row) and light phantom (lower row). MC modeling is performed with the optical properties similar those presented in Table 1 for phantom I and II respectively. Both phantoms have roughness 34 microns.

The results of MC modelling are well agreed both quantitatively and qualitatively with the results of experiment that is illustrated in Figure 5.

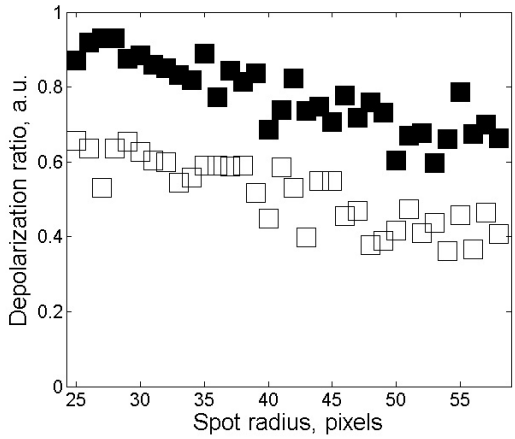

Figure 5. The profile of the radial distributions of depolarization ratio shown in Figure 4 for phantom I (Light) and phantom II (Dark) obtained by MC modeling, presented correspondingly to the results presented in Figure 3. Optical properties are presented in Table 1. The roughness in the simulation was 34 microns for both phantoms.

3.4 Depolarization ratio vs. surface roughness

In addition to the computational and experimental studies mentioned above the depolarization ratio vs. surface roughness was measured and calculated for light and dark phantoms in the case of free-speckle shown on Figure 6. The trend line connecting experimental points shown on Fig.6(a) as a solid line. We calculate the average depolarization ratio for radial distributions $D(R)$ by formula (12) and plot the experimental points for all 7 roughness on Fig.6(b).

$$\overline{D} = \frac{1}{N}\sum_{1}^{N} | D(R) | , \tag{12}$$

where N is the number of radial pixels. In our case we use N=150 pixels. Note, that finding the best classifier for the tissue separation using the radial distribution of D is not a scope of this paper. We plan to address this problem later. However, as one can see in Figure 6 using the average from (12) essentially increases the separation for every roughness compare to the free-space average depolarization calculated by (2).

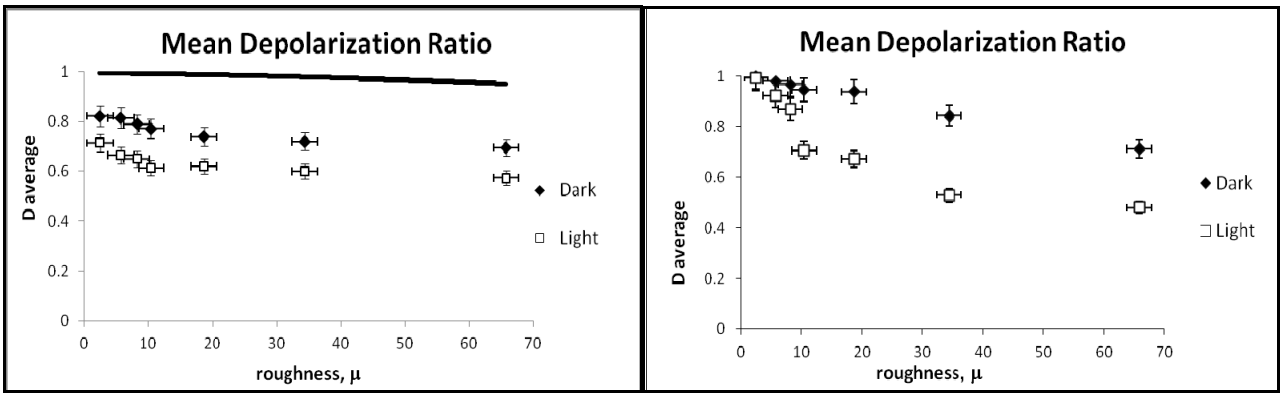

Figure 6. The experimental residual linear polarization for the dark and light skin phantoms(a) free space,(b) image .The solid line represents the depolarization by the metal surfaces.

The bulk scattering causes a strong light depolarization for all phantoms. For the particular phantom roughness also seriously decreases the residual polarization. The pair dark-light phantom with the close absorption but different scattering could be reliably separated at skin-like roughness by depolarization ratio. The phantom with the bigger reduced scattering coefficient (light) depolarizes light stronger than the phantoms with the smaller reduced scattering coefficient (dark). The coefficients of variation for each pair of experimental points are present in Table 2. Using the image speckle instead of free-speckle we could double the resolution between the phantoms.

Table 2. The coefficients of variation for each pair of experimental points.

Roughness, μm	Free-space speckle	Image speckle
10	11%	15%
19	9 %	17%
34	9%	23%
66	10%	19%

4. SUMMARY AND CONCLUSIONS

In this study we exploit whether the image speckle could improve skin cancer diagnostic in comparison with the previously used free-space speckle. The study includes the creation the skin phantoms of various roughness, measurements of co- and cross- polarized components of the back-scattered light, its analysis and computer modeling. To characterize the depolarization of light we measure the spatial distribution of speckle patterns and analyse their depolarization ratio taken into account radial symmetry. We examine the dependences of depolarization ratio vs. roughness for phantoms which optical properties are of the order of skin lesions. We demonstrate that the variation in bulk optical properties initiates the assessable changes in the depolarization ratio. We show that image speckle

differentiates phantoms significantly better than free-space speckle. The developed speckle pattern texture analysis approach allows obtaining information about surface roughness directly from the speckle pattern texture images using simple signal processing procedure presented above. Information extraction from the texture image is based on second-order statistics that has a strong correlation with the surface roughness. The results of experimental measurements are well agreed with the results of MC model developed in house. The developed MC tool can be used for direct simulation of light scattered by the skin phantoms of various roughness. The geometry of a particular probe and actual profile of the skin surface can be taken into account in these simulations. Therefore, we believe that developed and presented here both the MC technique and a new laser speckle-based experimental approach will find a number of new straightforward applications related to the non-invasive optical diagnostics of skin.

ACKNOWLEDGEMENTS

This work was supported in part by grants from the Canadian Dermatology Foundation, Canadian Institutes of Health Research, Natural Sciences and Engineering Research Council of Canada, UBC & VGH Hospital Foundation, and UBC Faculty of Medicine.

REFERENCES

[1] Tuchin, V.V., [Handbook of Coherent-Domain Optical Methods. Biomedical Diagnostics, Environmental Monitoring and Material Science], Springer Ney York (2012).
[2] Studninski, R.C.N. and Vitkin, I.A., "Methodology for examining polarized light interactions with tissues and tissuelike media in the exact backscattering direction," J. Biomed. Opt. 5(3), 330-337 (2000).
[3] Tuchin, V.V., Wang, L.V., and Zimnyakov, D.A., [Optical Polarization in Biomedical Applications], Springer, 111-138 (2006).
[4] Ghosh, N. and Vitkin, I.A., "Tissue polarimetry: concepts, challenges, applications, and outlook," J. Biomed. Opt. 16 (11), 110801 (2011).
[5] Rojas-Ochoa, L., Lacoste, D., Lenke, R., Schurtenberger, P., and Scheffold, F., "Depolarization of backscattered linearly polarized light," J. Opt. Soc. Am. A 21, 1799-1804 (2004).
[6] Angelsky, O.V., Ushenko, A.G., Ushenko, Y.A., Ushenko, Y.G., Tomka Y.Y. and Pishak V.P., "Polarization-correlation mapping of biological tissue coherent images," J. Biomed. Opt. 10, 064025 (2006).
[7] Takeda M., Wang W., and Hanson, S.G., "Polarization speckles and generalized Stokes vector wave: a review," Proc. SPIE 7387, 73870V (2010).
[8] Tchvialeva, L., Dhadwal, G., Lui, H., Kalia, S., Zeng, H., McLean, D.I., and Lee, T.K., "Polarization speckle imaging as a potential technique for *in vivo* skin cancer detection," J. Biomed. Opt. 18(6), 061211 (2012).
[9] Zerrad, M., Sorrentini, J., Soriano, G., Amra, C., "Gradual loss of polarization in light scattered from rough surfaces: Electromagnetic prediction," Opt. Express 18, 15832-15843 (2010).
[10] Tchvialeva, L., Markhvida, I., McLean, D.I., Lui, H., Zeng, H., and Lee, T.K., "Eliminating the effect of bulk scattering when measuring skin surface roughness using speckle contrast: a skin phantom study," Proc. SPIE 8230, 823004 (2012).
[11] Meglinski, I., and Doronin, A., " Monte Carlo modeling of photon migration for the needs of biomedical optics and biophotonics," [Advanced Biophotonics: tissue optical sectioning], Edited by R.K. Wang, V.V. Tuchin, Taylor & Francis, 1-72 (2014).
[12] Doronin, A., and Meglinski, I., "Online object oriented Monte Carlo computational tool for the needs of biomedical optics," Biomed. Opt. Express 9, 2461–2469 (2011).
[13] Kirillin, M., Meglinski, I., Sergeeva, E., Kuzmin, V.L., and Myllyla, R., "Simulation of optical coherence tomography images by Monte Carlo modeling based on polarization vector approach," Opt. Express 18, 21714–21724 (2010).
[14] Kuzmin, V.L., and Meglinski, I.V., "Coherent effects of multiple scattering for scalar and electromagnetic fields: Monte-Carlo simulation and Milne-like solutions," Opt. Commun. 273, 307–310 (2007).
[15] Kuzmin, V.L., and Meglinski, I.V., "Coherent multiple scattering effects and Monte Carlo method," JETP Lett. 79, 109–112 (2004).
[16] Tchvialeva, Zeng, H., Markhvida, I., McLean, D.I., L., Lui, H., and Lee, T.K., "Skin roughness assessment," [New Developments in Biomedical Engineering], Edited by Campolo, D., IN-TECH, 341-358(2010).
[17] Prahl, S., "Inverse Adding-Doubling," http://omlc.ogi.edu/software/iad/index.html (14 January 2014)

[18] Diao D., Tchvialeva L., Lui H., McLean D.I., and Lee T.K., "Durable rough skin phantoms for optical modeling," Phys. Med. Biol. 59(2), 485-492 (2014).
[19] Lister, T. and Chappell, P.H., "Optical properties of human skin," J. Biomed. Opt. 17(9), 090901 (2012).
[20] Meglinski, I.V., "Modeling the reflectance spectra of the optical radiation for random inhomogeneous multi-layered highly scattering and absorbing media by the Monte Carlo technique," Quantum Electron. 31, 1101–1107 (2001).
[21] Jacques, S.L., "Optical properties of biological tissues: a review," Phys. Med. Biol. 58(11), R37-R61 (2013).
[22] Garcia-Uribe A., Zou, J., Duvic, M., Cho-Vega, J.H., Prieto, V.G., and Wang, L.V., "*In vivo* diagnosis of melanoma and non-melanoma skin cancer using oblique incidence diffuse reflectance spectrometry," Cancer Res. 72(11), 2738-2745 (2012).
[23] Salomatina, E., Jiang, B., Novak, J., and Yaroslavsky, A.N., "Optical properties of normal and cancerous human skin in the visible and near-infrared spectral range," J. Biomed. Opt. 11(6), 064026 (2006).
[24] Doronin, A.V., Meglinski, I., "Peer-to-Peer Monte Carlo simulation of photon migration in topical applications of biomedical optics," J. Biomed. Opt. 17(9), 090504 (2012).
[25] Henyey, L., Greenstein, J., "Diffuse Radiation in the Galaxy," Astrophys. J. 93, 70-83 (1941).
[26] Churmakov, D.Y., Meglinski, I., Greenhalgh, D.A., "Influence of refractive index matching on the photon diffuse reflectance," Phys. Med. Biol. 47, 4271-4285 (2002).
[27] Zerrad, M., Sorrentini, J., Soriano, G., and Amra, C., "Gradual loss of polarization in light scattered from rough surfaces: Electromagnetic prediction," Opt. Exp. 18, 15832 (2010).
[28] van Rossum, M.C.W., Nieuwenhuizen, Th.M., "Multiple scattering of classical waves: microscopy, mesoscopy and diffusion," Rev. Mod. Phys. 71, 313-371 (1999).
[29] Akkermans, E., Montambaux, G., [Mesoscopic Physics of Electrons and Photons], Cambridge University Press, (2011).
[30] Kuzmin, V.L., Meglinski, I., "Numerical simulation of coherent back-scattering and temporal intensity correlations in random media," Quantum Electron. 36, 990-1002 (2006).